

# Mechanical Forces of Fission Yeast Growth

Nicolas Minc,<sup>1</sup> Arezki Boudaoud,<sup>2,\*</sup> and Fred Chang<sup>1,\*</sup>

<sup>1</sup>Department of Microbiology, Columbia University College of Physicians and Surgeons, 701 W 168<sup>th</sup> Street, New York, NY 10032, USA

<sup>2</sup>Laboratoire de Physique Statistique, Ecole Normale Supérieure, UPMC Paris 06, Université Paris Diderot, CNRS, 24 rue Lhomond, 75005 Paris, France

## Summary

Mechanical properties contribute to the control of cell size, morphogenesis, development, and lifestyle of fungal cells [1–4]. Tip growth can be understood by a viscoplastic model, in which growth is derived by high internal turgor pressure and cell-wall elasticity [2, 5]. To understand how these properties regulate growth in the rod-shaped fission yeast *Schizosaccharomyces pombe*, we devised femtoliter cylindrical polydimethylsiloxane (PDMS) microchambers with varying elasticity as force sensors for single cells. By buckling cells in these chambers, we determine the elastic surface modulus of the cell wall to be  $20.2 \pm 6.1 \text{ N.m}^{-1}$ . By analyzing the growth of the cells as they push against the walls of the chamber, we derive force-velocity relationships and values for internal effective turgor pressure of  $0.85 \pm 0.15 \text{ MPa}$  and a growth-stalling force of  $11 \pm 3 \mu\text{N}$ . The behavior of cells buckling under the force of their own growth provides an independent test of this model and parameters. Force generation is dependent on turgor pressure and a glycerol synthesis gene, *gpd1<sup>+</sup>* (glycerol-3-phosphate dehydrogenase), and is independent of actin cables. This study develops a quantitative framework for tip cell growth and characterizes mechanisms of force generation that contribute to fungal invasion into host tissues.

## Results and Discussion

### Viscoplastic Model for Fission Yeast Tip Growth

A mechanical view of fungal tip growth can be explained in terms of a viscoplastic model, which has been proposed previously to describe mechanisms of cell-shape control and growth in large green algae and plant cells [2, 3, 5–8]. In this model, a high turgor pressure produces the work necessary to deform the new cell wall deposited at cell tips. Growth appears effectively as a viscoplastic process: At a critical value of the pressure,  $P_c$ , the wall reaches a threshold strain (the plastic yield strain) and is deformed irreversibly. The growth rate of the cell,  $v_0$ , is proportional to the strain in the wall in excess of this threshold, so that

$$v_0 \propto \frac{(P - P_c)}{E_{cw}}, \quad (\text{Equation 1})$$

in which  $E_{cw}$  is the Young's elastic modulus of the wall and  $P$ , the total turgor pressure (Figure 1A; see Supplemental Data,

available online). Here, we provide a test of this mechanical view by experimentally measuring the key parameters and assessing the effect of external forces on growth rates.

### Microfabricated PDMS Chambers as Force Sensors for Single Cells

We devised microfabricated polydimethylsiloxane (PDMS) chambers as single-cell force sensors for fission yeast cells. Previous approaches used for measuring mechanical properties of diverse fungi include assaying the effects of extracellular osmolarity [1, 9, 10], the ability of a cell to penetrate or pierce materials [1, 11], strain gauges and waveguide microscopy, and atomic force microscopy (AFM) [1, 12–16]. On the whole, however, definitive quantitative data for these parameters have been lacking, given the significant discrepancies between many of these approaches, as well as caveats and technical complexities associated with each.

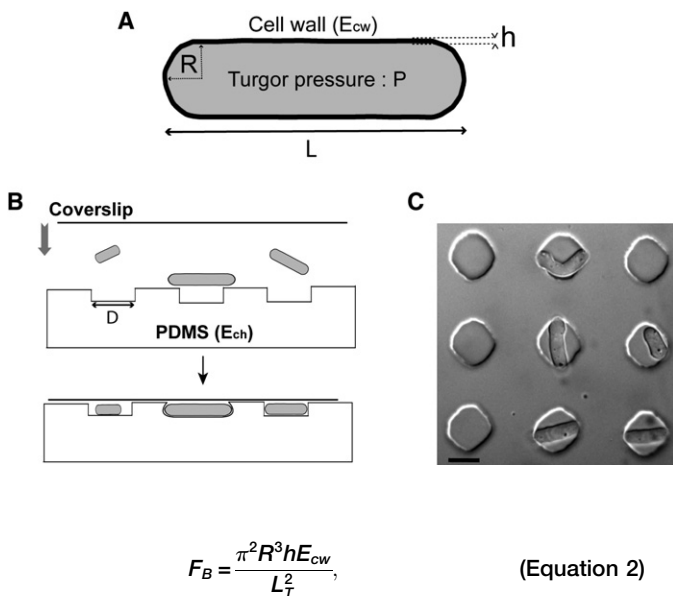
PDMS arrays contained about 10,000 microfabricated cylindrical chambers, 5  $\mu\text{m}$  deep and with a diameter,  $D$ , ranging from 10 to 50  $\mu\text{m}$  [17]. We varied the elasticity (Young's modulus,  $E_{ch}$ ) of the PDMS from 0.1 to 1.5 MPa by adjusting the ratio of polymer versus cross-linker (Figure S1). Fission yeast cells were placed between the PDMS array and a glass coverslip and pushed into the chambers by a slight pressing of the coverslip (Figures 1B and 1C). We analyzed cells of lengths from approximately 8 to 25  $\mu\text{m}$  by using a *cdc25-22* mutant at 25°C, which grows longer than wild-type cells because of a cell-cycle delay in the G2 phase. The radius of the cell is largely insensitive to these changes in length and remains around 2  $\mu\text{m}$  [18]. We analyzed, as controls, cells that were placed in larger chambers in which they did not contact the sides of the chambers (Movie S1). In general, cells that were bent or growing against the edge of the chamber continued to divide in the cell cycle. To test whether the stress-response pathways are induced in these bent cells, we monitored the stress reporters *sty1*-green fluorescent protein (GFP) and *pap1*-GFP, which relocalize from the cytoplasm to the nucleus in the presence of osmotic or oxidative stress [19–21]. We noted no marked change in the distribution of these markers when the cells were growing under constraint or even when they were buckling (Figure S2), indicating that these conditions do not cause high levels of cell stress.

### Measuring Cell-Wall Elasticity

We first sought to estimate the elasticity of the cell wall. In these experiments, we pushed the cells into chambers smaller than the length of the cells. In general, in stiff chambers, cells were immediately bent in the chamber, whereas in softer chambers, the cell deformed the chamber (Figure 2A). As an illustration of the elasticity of the cell wall, in rare cases, cells were observed to pop out of the well and straighten out within seconds, even after being repeatedly pushed back into the well (Movie S2).

The deformation of the chamber by the cell provided a measurement of the elasticity of the cell wall. For this measurement, we used the buckling transition from a straight shape to a bent shape; this transition is induced by the longitudinal forces exerted by the chamber on the cell. The threshold force for buckling is given by

\*Correspondence: boudaoud@ips.ens.fr (A.B.), fc99@columbia.edu (F.C.)



with  $L_T$  the distance between cell tips along the force axis,  $R$  the cell's radius, and  $h$  the cell-wall thickness (see [Supplemental Data](#) and [22]). Note that turgor pressure is not included in this equation because it is compensated by the tension in the wall. The deformation of the chamber (Figure 2B),  $d = L_T - D$ , concomitantly provides a measurement of the force,  $F$ , exerted by the cell on the chamber (see [Supplemental Data](#)):

$$F = \frac{8}{3} E_{ch} R d. \quad (\text{Equation 3})$$

The balance of forces,  $F_B = F$ , leads to

$$d = \left( \frac{3\pi^2}{8} \frac{R^2}{(D+d)^2 E_{ch}} \right) E_{cw} h = \frac{E_{cw} h}{E^*}, \quad (\text{Equation 4})$$

Figure 1. Microfabricated Chambers as Single-Cell Force Sensors for Studying the Mechanical Properties of Fission Yeast Cells

(A) Parameters of a fission yeast cell. The cell-wall layer has an elastic modulus,  $E_{cw}$ , and a thickness  $h$ . The turgor pressure inside the cell is  $P$ . The rod-shaped cell has a radius  $R$  and a length  $L$ .

(B) Schematic showing how yeast cells are placed into the PDMS chambers.

(C) Top-view image of an array of chambers with cells inside. Scale bar represents  $10 \mu\text{m}$ .

in which we introduced  $E^*$  as a rescaled elastic modulus for the chamber. This relation allows for computing the surface modulus of the cell wall,  $\sigma_{cw} = E_{cw} h$  (Figure 2B).

We measured the behavior of cells of varying length in chambers of varying diameters and elasticity, allowing us to vary  $d$  and  $E^*$  by an order of magnitude. Figure 2C depicts measurements of 155 cells. Although we obtained a good linear scaling between  $d$  and  $(E^*)^{-1}$  at small deformation, saturation was noted at very high deformation; this property may arise from a nonlinear elastic response of the material (Figure S1B). We thus used a second-order polynomial fit, in which the linear term corresponds to the surface modulus, and obtained  $\sigma_{cw} = 20.2 \pm 6.1 \text{ N}\cdot\text{m}^{-1}$ . Given that the thickness of the fission yeast cell wall ( $h$ ) has been measured by electron microscopy to be around  $200 \text{ nm}$  [23], our measurements estimate the Young's elastic modulus of the fission yeast cell wall to be:  $E_{cw} = 101 \pm 30 \text{ MPa}$ .

This elastic modulus was independent of cell length (correlation coefficient:  $R^2 = 0.07$ ) and did not vary significantly between interphase and mitotic cells. We note that this measurement corresponds to the elasticity of the side wall in this buckling experiment. However, we predict that although the elasticity of the cell tips may be slightly softer than this measured value to account for localized cell growth, it is likely to be similar to the measured value, as demonstrated by the near-uniform response of the cell wall to osmotic

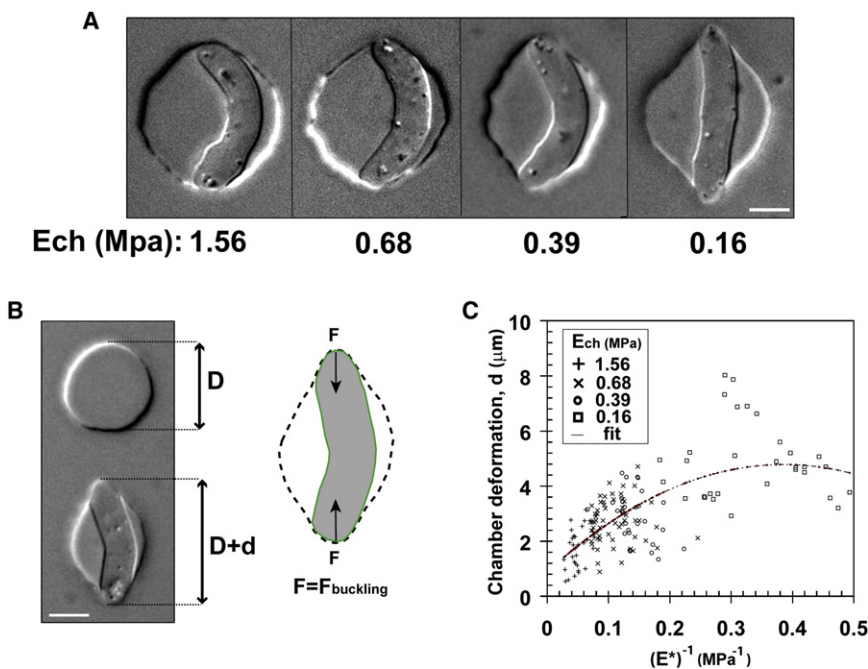


Figure 2. Measuring Fission Yeast Cell-Wall Elastic Modulus

(A) Single fission yeast cells with similar cell lengths were pushed into chambers smaller than the cells. Chambers with decreasing elastic moduli  $E_{ch}$  (from left to right) are shown. Scale bars represent  $5 \mu\text{m}$ .

(B) Illustration of the method used to compute chamber deformation. (Left) The initial chamber diameter,  $D$ , is measured on the surrounding chambers (precision better than 5%), and the deformation,  $d$ , is measured along the force axis. (Right) The force from the chamber deformation equilibrates the buckling force. Because this buckling force is proportional to the cell-wall surface modulus, this method allows for a direct calculation of the cell-wall surface modulus at the single-cell level. Scale bar represents  $5 \mu\text{m}$ .

(C) Plot of the chamber deformation as a function of the inverse of the scaled chamber elastic modulus ( $E^*$ , see Equation 4) obtained from 155 single cells. Different symbols correspond to different chamber elastic moduli, as shown in the legend. The fit used is parabolic to account for second-order saturations at larger deformation. The imprecision in the measurement is found to be higher than the scattering of the data around the proposed fit. The strain is NM11.

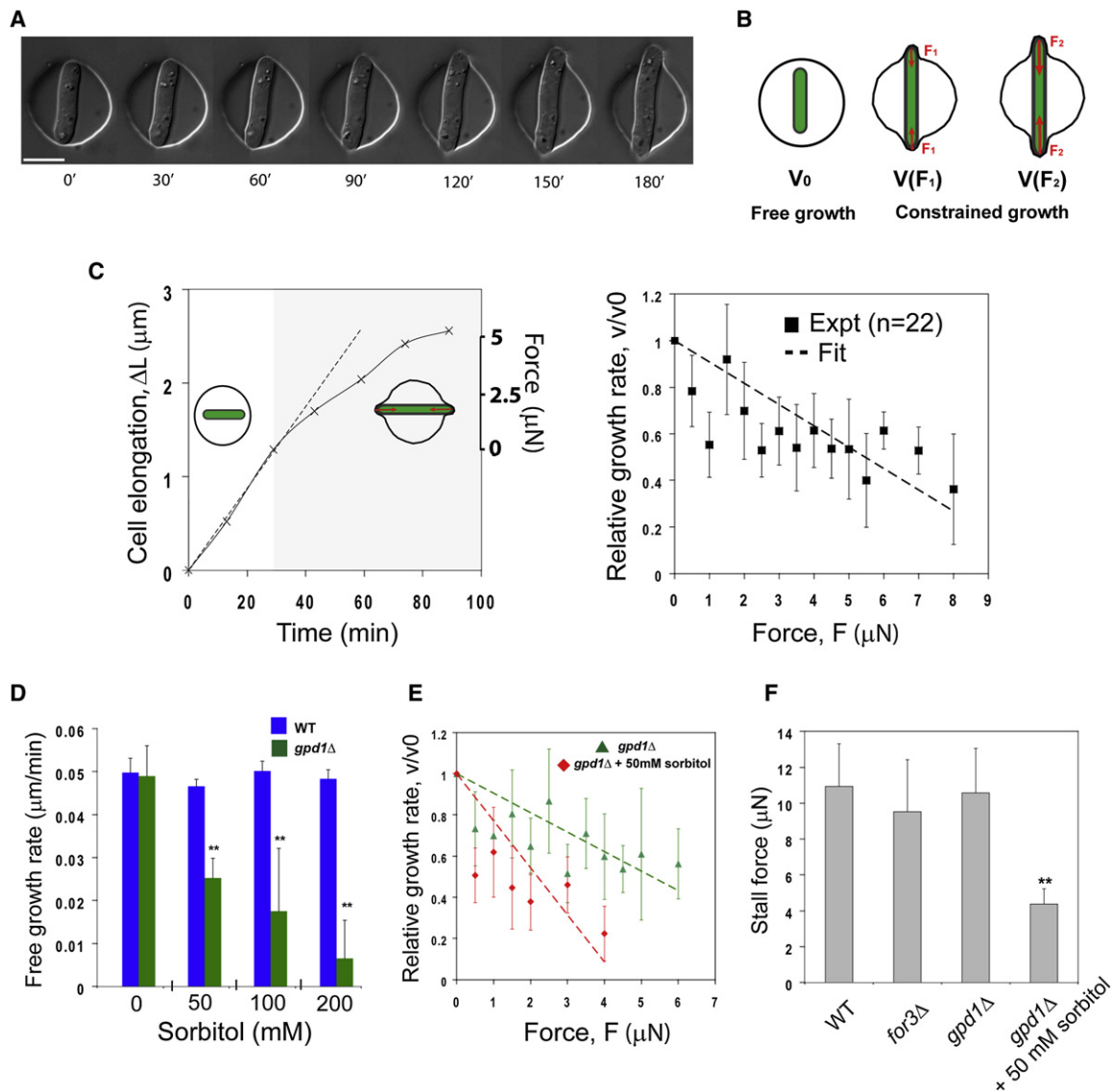


Figure 3. Force-Velocity Relations for Fission Yeast Cell Growth

(A) Time-lapse sequence of a fission yeast cell growing in and deforming a chamber made of soft PDMS (elastic modulus,  $E_{ch} = 0.16$  Mpa). Scale bar represents  $10 \mu\text{m}$ .

(B) Schematic illustrating the basis of the experiments. The free growth rate,  $v_0$ , is measured before the cell is deforming the chamber. When the cell deforms the chamber, the force from the deformation opposes turgor and may reduce the growth rate,  $v(F)$ . As the cell deforms the chamber more and more, the force increases ( $F_2 > F_1$ ), which may continue changing the growth rate.

(C) Cell growth under an external force. (Left) Example of growth curve of a single cell growing in a stiff chamber ( $E_{ch} = 0.65$ MPa). The dotted lines follow the free growth rate as measured before contact. The gray part highlights the phase of growth under external force. The left axis plots the cell elongation:  $\Delta L = L(t) - L(t = 0)$ . The right axis plots the external force of the deformed chamber. (Right) Force-velocity plot. Each point is averaged on typically 3–4 different experimental sets, and forces are binned so that a sample size is kept almost constant. The vertical error bars represent the standard deviations. The dotted line plots a linear fit that corresponds to Equation 5.

(D) Free growth rate measured in bipolar wild-type and *gpd1Δ* cells in the presence of increasing concentrations of sorbitol (0, 0.05, 0.1, and 0.2 M).  $n = 10$  cells for each condition.

(E) Force-velocity plot of *gpd1Δ* cells in the absence and in the presence of 0.05 M sorbitol.  $n = 15$  cells in both conditions.

(F) Stalling forces extrapolated from force-velocity curves in the indicated mutants and conditions. The yeast strains are: NM11, NM183, and NM209 (all in a *cdc25-22* background and grown at 25°C). Double asterisks represent a Student's t test,  $p < 0.005$ .

shock or when pushing against the wall of the chamber (see below).

### Force-Velocity Relationships of Cell Growth

Next, we sought to measure the force exerted by the growth of single cells, using the chambers of varying stiffness as force sensors. In principle, the maximum force of cell growth can

be estimated by measuring the external force required to stall growth, the “stall force.” In these experiments, we introduced into the chambers cells that were initially shorter than the diameter of the chamber. Over time, the cells elongated, and when both cell ends contacted the wall of the chamber, the cells pushed against the chamber (Figure 3A and Movie S3). Because growth patterns change over the cell cycle, we

focused our analysis on only interphase cells growing from both cell tips in a bipolar manner [18]. Depending on the stiffness of the PDMS, the growth of the cells often deformed the chamber from a round shape into an oval shape (or a “Phi  $\Phi$ ” shape). The force exerted by the chamber increased as the chamber was progressively deformed, much like a spring being stretched. The different rates of growth of the cell and deformation of the chamber provided a measurement of a force-velocity relationship. We established this relation by tracking growth rates before (free growth =  $v_0$ ) and after (constrained growth =  $v$ ) the cell began to deform the chamber, at different forces ( $F$ ) (Figure 3B). After the cell began to deform the chamber, we observed a clear decrease in growth rate (Figure 3C). The corresponding force-velocity relationship obtained from tracking 22 individual cells depicted a gradual decrease in growth rates as the external force was increasing (Figure 3C). The external force of the chamber may oppose turgor stress on the cell wall, which leads to an artificial reduction of the effect of turgor and a reduction of the growth rate (see Supplemental Data), so that

$$\frac{v(F)}{v_0} = \left(1 - \frac{F}{\pi R^2 \Delta P}\right). \quad (\text{Equation 5})$$

Here,  $\Delta p = P - P_c$  is the effective turgor pressure (Equation 1). Note that we could not experimentally measure a stall force, because this force is typically higher than the buckling force; cells usually buckled before stalling, which allowed growth to resume (Movie S4; see below). However, by linearly fitting the experimental data and extrapolating the fit to  $v(F) = 0$ , we could derive an estimate of the stalling force to be  $11 \pm 3 \mu\text{N}$ .

#### Growth Rates and Forces Depend on Internal Turgor Pressure

Next, we tested the role of turgor pressure on force production. We predicted that increasing the extracellular osmolarity in the media would cause a relative decrease in internal turgor pressure and, thus, a decrease in force production. However, wild-type cells have a complex compensatory osmotic-stress response: when osmolarity of the external media is increased by the addition of sorbitol, wild-type cells initially shrink, but they then recover their initial turgor values within 10–30 min [24] (Movie S5). This recovery is dependent on the synthesis of intracellular glycerol, which is catalyzed by the enzyme *gpd1p* (glycerol-3-phosphate dehydrogenase) [25–27] (Movie S6). The *gpd1Δ* mutant cell is viable, because *gpd1+* shares some functional redundancy with a second glycerol-3-phosphate dehydrogenase gene, *gpd2+* (data not shown, [24]), but is sensitive to hyperosmotic medium. Thus, to avoid most of the complex dynamic effects of stress regulation, we examined the effects of altering osmolarity of the media in *gpd1Δ* mutant cells.

First, we incubated cells in different concentrations of sorbitol and monitored free-growth rates in the subsequent 2 hr. We found that *gpd1Δ* mutants grew significantly slower at 0.05 M sorbitol and stopped growing at sorbitol concentrations exceeding 0.2 M. Under the same conditions, wild-type cells did not exhibit any notable change in their growth rate (Figure 3D).

Second, we examined the force-velocity behavior of *gpd1Δ* mutants growing in chambers. In the absence of sorbitol, *gpd1Δ* cells did not show significant differences in behavior in comparison to wild-type cells (Figure 3E and Figure S3B). In contrast, *gpd1Δ* cells in 0.05 M sorbitol exhibited a force-

velocity curve with a significantly smaller slope; the derived stalling force of this mutant was typically 2–3 times lower than that observed in the absence of sorbitol (Figures 3E and 3F). Thus, in these conditions, *gpd1Δ* mutant cells, which are defective in turgor-pressure regulation, produce less force. These results support a view that internal turgor pressure, regulated by intracellular glycerol concentration, controls cell-growth rates and force production.

#### Growth Force Is Independent of Actin Cables

Because the actin cytoskeleton is critical for force generation in the migration of animal cells [28], we also tested whether actin affects force production in *S. pombe*. In interphase cells, actin is organized in actin cables, which regulate polarized cell growth, and actin patches, which are involved in endocytosis. Although total inhibition of F-actin by Latrunculin A immediately halts growth, possibly through many indirect effects, we probed the role of actin cables by examining *for3Δ* cells, which lack actin cables but still exhibit polarized cell growth [29]. Interestingly, in our assays, *for3Δ* cells did not show any major difference in comparison to wild-type cells. Free-growth rate and force-velocity behavior were similar, and the stalling force of *for3Δ* cells was not significantly smaller than that of wild-type cells (Figure 3F and Figure S3B). Thus, these findings show that actin cables are not required for force production.

#### Cells Buckle from the Force of Their Own Growth

As an independent test of our measurements and model, we investigated the behavior of cells that buckle in chambers from the force of their own growth. We grew cells in very stiff chambers ( $E_{\text{ch}} = 1.55 \text{ MPa}$ ) that are mostly undeformed by the cells. When cells elongated to the walls of the chamber, they grew and buckled under their own pushing force (Figure 4A and Movie S7). The buckling event usually happened quite abruptly, in a time as short as 5 min (see the rate of angle change between the tips in Figure 4B). In a subset of cells that buckled and later divided, we could observe that the two daughter cells recovered immediately in a straight shape (Movie S8).

Growth curves revealed that when cells reached the side of the chamber, growth slowed down and then stopped for a reproducible time period before buckling occurred (Figure 4B). By analyzing cells of different lengths, we saw that the delay before buckling,  $\Delta t$ , was inversely correlated with cell length (Figures 4B and 4C).

These experiments provided us with an independent way to test our measurements from the previous experiments. On the one hand, if the elasticity of the cell wall is known, the buckling event provides a value of the external force,  $F = F_B$  (Equation 2), at the moment of buckling. On the other hand, we could obtain the evolution of the force before buckling from our growth law (Supplemental Data). Plugging the values obtained from the first sets of experiments ( $E_{\text{cw}}, \Delta P$ ) into a model adapted to these dynamic buckling experiments allowed us to compare the experimental data to their theoretical counterparts (Figure 4C and Supplemental Data). The overall agreement obtained was found to be within the range of error in our measurements. Thus, this analysis provides an independent confirmation of the values of the mechanical parameters and supports our model for cell growth.

In summary, we have introduced a novel, simple approach for studying mechanical aspects of living cells by using microchambers. The general experimental and theoretical approaches could be adapted to many walled cell types. The

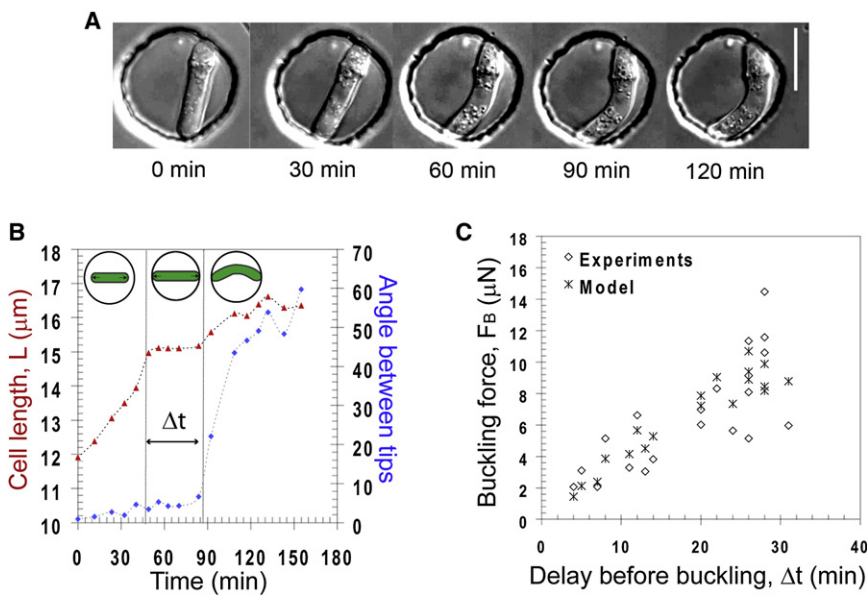


Figure 4. Cell Buckling under Its Own Pushing Force

(A) Time-lapse sequence of a fission yeast cell growing and buckling under its own pushing force in a rigid chamber. Scale bar represents 10  $\mu\text{m}$ . (B) Example of a growth curve of a cell buckling in a 15  $\mu\text{m}$  chamber. The delay,  $\Delta t$ , during which the cell length stalls is indicated. The angle between cell tips represented on the right axis in blue is used for detection of the onset of buckling. (C) Buckling force,  $F_B$ , plotted as a function of the delay,  $\Delta t$ , along with values predicted from the model. The yeast strains are NM11 and FC1234.

### Experimental Procedures

#### Chamber Microfabrication

Microchambers were fabricated by the use of standard soft-lithography methods [35]. Chambers are cylindrical, 5  $\mu\text{m}$  deep, and have diameters varying between 10 and 50  $\mu\text{m}$  (10, 12, 15, 20, 25, 30, 35, 40, and 50  $\mu\text{m}$ ). PDMS of varying elastic moduli were generated by using different ratios of polymer versus crosslinker (see Figure S1) and baking the mixture for 4 hr at 65°C. The corresponding values of the elastic moduli were calculated by pulling on a large PDMS rectangle (typically 20  $\times$  50  $\times$  100  $\text{mm}^3$ ) with increasing forces and measuring the deformation in length along the force axis. The value was computed by

$$\frac{\Delta L}{L} = \frac{F}{E_{ch}s}$$

in which  $s$  is the cross-section area and  $L$  is the length of the rectangle. The PDMS chambers were activated with the use of a plasma cleaner (Harrick Plasma, Ithaca, NY, USA).

#### Microscopy and Image Analysis

Microscopy was performed at room temperature (23°C–27°C) with an inverted microscope provided with a motorized stage (Ludl Electronic Products, Hawthorne, NY, USA). For force-velocity relations establishment, each typical experimental set was performed with the use of a motorized stage so that 10–15 movies could be performed for each set. Cells growing in a bipolar manner were selected by tracking the growth from each tip relative to a fixed fiduciary mark (a birthscar) on the cell wall. GFP-tubulin and calponin homology domain (CHD)-GFP confocal stacks were performed on a spinning-disk confocal fluorescent microscope. Images were acquired with OpenLab 4.0.4 (Improvision) and processed and analyzed with Image J (NIH) and Matlab (Mathworks).

#### Yeast Strains, Media, and Genetic Methods

Standard methods for *S. pombe* media and genetic manipulations were used (<http://www-rcf.usc.edu/~forsburg/>). Strains used in this study are listed in Table S1. Cells were grown to exponential phase in YE5S liquid media at 25°C before being placed into the chambers. GFP-labeled tubulin was used for monitoring the stage of the cell cycle, and the *cdc25-22* mutation was used in slightly delaying the G2 stage of the cell cycle for the production of cells with longer lengths. Chambers were incubated at room temperature of approximately 23°C–27°C. Hydroxyurea (HU), employed in Figure 4, was used at a final concentration of 25 mM from a 60X stock solution in water and was added to the cell 2 hr before the experiment.

#### Supplemental Data

Supplemental Data include a detailed description of the theoretical model, four figures, one table, and eight movies and can be found with this article online at [http://www.cell.com/current-biology/supplemental/S0960-9822\(09\)01132-4](http://www.cell.com/current-biology/supplemental/S0960-9822(09)01132-4).

#### Acknowledgments

The authors acknowledge all members of the Chang laboratory for discussions and technical assistance. We thank O. Rossier, the M. Sheetz

measurements of the cell-wall surface modulus have a resolution on the order of 1  $\text{N}\cdot\text{m}^{-1}$  and should be valid up to 50  $\text{N}\cdot\text{m}^{-1}$ . The external forces can typically be resolved within 0.5  $\mu\text{N}$  and may be measured at values reaching 50–70  $\mu\text{N}$ .

The present study supports a view that polarized cell growth in fission yeast is driven by high internal turgor pressure that is partially contained by a stiff but elastic cell wall. The elastic modulus measured of  $E_{cw} = 101 \pm 30 \text{ MPa}$  is globally similar to previously reported values of other fungi cell walls measured by other means: 110  $\pm 10 \text{ MPa}$  for *A. nidulans* [30] and 112  $\pm 6 \text{ MPa}$  for *S. cerevisiae* [13]. This stiffness is similar to that of rubber. The effective turgor pressure that drives growth is about 0.85 MPa. This may correspond to a total turgor pressure around 0.95 MPa (see Supplemental Data). The osmotic potential corresponding to this turgor pressure would be generated by a concentration of about 0.4 M glycerol. This globally corresponds to the concentration of external sorbitol at which the cell starts to notably shrink (data not shown). Finally, these mechanical measurements coupled with mathematical models may begin to provide insights into cell-size determination [2].

The derived stall force suggests that the growing cell tip is able to resist forces of up to 11  $\mu\text{N}$ , yielding a stalling pressure of about 1  $\mu\text{N}\cdot\mu\text{m}^{-2}$ . This corresponds to the force experienced by a palm of a hand holding approximately 100–300 kg, illustrating the considerable strength exerted by these microbial cells. As a comparison, the forces generated at the leading edge of migrating animal cells is 100–1000 times less, on the order of 10–100 nN [31].

Mechanical forces are likely to be key factors in fungal pathogenesis [1]. Plant pathogen fungi form appressoria structures, which raise turgor pressure to breach the plant cell wall for host invasion [32]. *Candida albicans* can pierce through the membranes of macrophages [33, 34]. There has been a question of whether fungi invade host membranes by using mechanical force, as opposed to more chemical mechanisms. The mechanical resistance of cutaneous tissue is typically on the order of 1–10  $\mu\text{N}\cdot\mu\text{m}^{-2}$  [1]. Our measurements of a similar magnitude suggest that the impressive mechanical growth forces from the fungal tip can be a major factor in driving host invasion.

laboratory, and the J. Dworkin laboratory for technical support, as well as F. Corson, T. Lionnet, and P. Meyer for insightful discussions. We are grateful to E. Hidalgo, H. Aiba, and S. Martin for strains. Microfabrication was made in the Columbia CEPSPR clean room. This work was supported by National Institutes of Health (NIH) grant GM056836.

Received: October 24, 2008

Revised: April 14, 2009

Accepted: May 5, 2009

Published online: June 4, 2009

## References

1. Bastmeyer, M., Deising, H.B., and Bechinger, C. (2002). Force exertion in fungal infection. *Annu. Rev. Biophys. Biomol. Struct.* **31**, 321–341.
2. Boudaoud, A. (2003). Growth of walled cells: from shells to vesicles. *Phys. Rev. Lett.* **91**, 018104.
3. Harold, F.M. (1990). To shape a cell: an inquiry into the causes of morphogenesis of microorganisms. *Microbiol. Rev.* **54**, 381–431.
4. Slaughter, B., and Li, R. (2006). Toward a molecular interpretation of the surface stress theory for yeast morphogenesis. *Curr. Opin. Cell Biol.* **18**, 47–53.
5. Lockhart, J.A. (1965). An Analysis of Irreversible Plant Cell Elongation. *J. Theor. Biol.* **8**, 264.
6. Green, P.B., Erickson, R.O., and Buggy, J. (1971). Metabolic and Physical Control of Cell Elongation Rate - in-Vivo Studies in *Nitella*. *Plant Physiol.* **47**, 423.
7. Proseus, T.E., Ortega, J.K.E., and Boyer, J.S. (1999). Separating growth from elastic deformation during cell enlargement. *Plant Physiol.* **119**, 775–784.
8. Dumais, J., Shaw, S.L., Steele, C.R., Long, S.R., and Ray, P.M. (2006). An anisotropic-viscoplastic model of plant cell morphogenesis by tip growth. *Int. J. Dev. Biol.* **50**, 209–222.
9. Money, N.P. (1997). Mechanism linking cellular pigmentation and pathogenicity in rice blast disease. *Fungal Genet. Biol.* **22**, 151–152.
10. Lew, R.R., Levina, N.N., Walker, S.K., and Garrill, A. (2004). Turgor regulation in hyphal organisms. *Fungal Genet. Biol.* **41**, 1007–1015.
11. Howard, R.J., Ferrari, M.A., Roach, D.H., and Money, N.P. (1991). Penetration of hard substrates by a fungus employing enormous turgor pressures. *Proc. Natl. Acad. Sci. USA* **88**, 11281–11284.
12. Touhami, A., Nysten, B., and Dufrene, Y. (2003). Nanoscale mapping of the elasticity of microbial cells by atomic force microscopy. *Langmuir* **19**, 4539–4543.
13. Smith, A.E., Zhang, Z., Thomas, C.R., Moxham, K.E., and Middelberg, A.P. (2000). The mechanical properties of *Saccharomyces cerevisiae*. *Proc. Natl. Acad. Sci. USA* **97**, 9871–9874.
14. Dufrene, Y.F. (2008). Towards nanomicrobiology using atomic force microscopy. *Nat. Rev. Microbiol.* **6**, 674–680.
15. Bechinger, C., Giebel, K.F., Schnell, M., Leiderer, P., Deising, H.B., and Bastmeyer, M. (1999). Optical measurements of invasive forces exerted by appressoria of a plant pathogenic fungus. *Science* **285**, 1896–1899.
16. Money, N.P., Davis, C.M., and Ravishankar, J.P. (2004). Biomechanical evidence for convergent evolution of the invasive growth process among fungi and oomycete water molds. *Fungal Genet. Biol.* **41**, 872–876.
17. Minc, N., Bratman, S.V., Basu, R., and Chang, F. (2009). Establishing new sites of polarization by microtubules. *Curr. Biol.* **19**, 83–94.
18. Mitchison, J.M., and Nurse, P. (1985). Growth in cell length in the fission yeast *Schizosaccharomyces pombe*. *J. Cell Sci.* **75**, 357–376.
19. Castillo, E.A., Ayte, J., Chiva, C., Moldon, A., Carrascal, M., Abian, J., Jones, N., and Hidalgo, E. (2002). Diethylmaleate activates the transcription factor Pap1 by covalent modification of critical cysteine residues. *Mol. Microbiol.* **45**, 243–254.
20. Gaits, F., Degols, G., Shiozaki, K., and Russell, P. (1998). Phosphorylation and association with the transcription factor Atf1 regulate localization of Spc1/Sty1 stress-activated kinase in fission yeast. *Genes Dev.* **12**, 1464–1473.
21. Zuin, A., Vivancos, A.P., Sanso, M., Takatsume, Y., Ayte, J., Inoue, Y., and Hidalgo, E. (2005). The glycolytic metabolite methylglyoxal activates Pap1 and Sty1 stress responses in *Schizosaccharomyces pombe*. *J. Biol. Chem.* **280**, 36708–36713.
22. Landau, L.D., and Lifshitz, E.M. (1959). *Theory of Elasticity* (Moscow: MIR).
23. Osumi, M. (1998). The ultrastructure of yeast: cell wall structure and formation. *Micron* **29**, 207–233.
24. Ohmiya, R., Yamada, H., Nakashima, K., Aiba, H., and Mizuno, T. (1995). Osmoregulation of fission yeast: cloning of two distinct genes encoding glycerol-3-phosphate dehydrogenase, one of which is responsible for osmotolerance for growth. *Mol. Microbiol.* **18**, 963–973.
25. Aiba, H., Yamada, H., Ohmiya, R., and Mizuno, T. (1995). The osmo-inducible *gpd1+* gene is a target of the signaling pathway involving Wis1 MAP-kinase kinase in fission yeast. *FEBS Lett.* **376**, 199–201.
26. Degols, G., Shiozaki, K., and Russell, P. (1996). Activation and regulation of the Spc1 stress-activated protein kinase in *Schizosaccharomyces pombe*. *Mol. Cell. Biol.* **16**, 2870–2877.
27. Hohmann, S. (2002). Osmotic stress signaling and osmoadaptation in yeasts. *Microbiol. Mol. Biol. Rev.* **66**, 300–372.
28. Gardel, M.L., Sabass, B., Ji, L., Danuser, G., Schwarz, U.S., and Waterman, C.M. (2008). Traction stress in focal adhesions correlates biphasically with actin retrograde flow speed. *J. Cell Biol.* **183**, 999–1005.
29. Feierbach, B., and Chang, F. (2001). Roles of the fission yeast formin for3p in cell polarity, actin cable formation and symmetric cell division. *Curr. Biol.* **11**, 1656–1665.
30. Zhao, L., Schaefer, D., Xu, H., Modi, S.J., LaCourse, W.R., and Marten, M.R. (2005). Elastic properties of the cell wall of *Aspergillus nidulans* studied with atomic force microscopy. *Biotechnol. Prog.* **21**, 292–299.
31. du Roure, O., Saez, A., Buguin, A., Austin, R.H., Chavrier, P., Silberzan, P., and Ladoux, B. (2005). Force mapping in epithelial cell migration. *Proc. Natl. Acad. Sci. USA* **102**, 2390–2395.
32. Emmett, R., and Parbery, D. (1975). Appressoria. *Annu. Rev. Phytopathol.* **13**, 147–167.
33. Gow, N.A., Brown, A.J., and Odds, F.C. (2002). Fungal morphogenesis and host invasion. *Curr. Opin. Microbiol.* **5**, 366–371.
34. Lo, H.J., Kohler, J.R., DiDomenico, B., Loebeberg, D., Cacciapuoti, A., and Fink, G.R. (1997). Nonfilamentous *C. albicans* mutants are avirulent. *Cell* **90**, 939–949.
35. Weibel, D.B., Diluzio, W.R., and Whitesides, G.M. (2007). Microfabrication meets microbiology. *Nat. Rev. Microbiol.* **5**, 209–218.